remote sensing

MDPI

Article

Impacts of the 2019–2020 Black Summer Drought on Eastern Australian Forests

Nuwanthi Arampola [1,2,*], Belinda Medlyn [1], Samuel Hislop [3], Brendan Choat [1], Stefan Olin [2], Ali Mansourian [2], Pengxiang Zhao [2] and Benjamin Smith [1,2]

[1] Hawkesbury Institute for the Environment, Western Sydney University, Richmond, NSW 2753, Australia; ben.smith@westernsydney.edu.au (B.S.)
[2] Department of Physical Geography and Ecosystem Science, Lund University, 223 62 Lund, Sweden
[3] Department of Geospatial Sciences, RMIT University, Melbourne, VIC 3000, Australia
* Correspondence: n.arampola@westernsydney.edu.au or nuwanthi.arampola@nateko.lu.se

Abstract: Droughts present a significant global challenge, particularly to forest ecosystems in regions such as eastern New South Wales, Australia, which is known for its dry climate and frequent, intense droughts. Recent studies have indicated a notable increase in tree mortality and canopy browning across this area, especially during the recent extreme drought period culminating in the Black Summer of 2019–2020. Our study investigates the impacts of drought on eucalypt forests by leveraging remote sensing and field observation data to detect and analyse vegetation health and stress indicators. Utilising data from Sentinel-2, alongside historical Landsat observations, we applied multiple spectral vegetation indices, namely the Normalized Difference Vegetation Index (NDVI), Normalized Difference Moisture Index (NDMI), Normalized Burn Ratio (NBR), and Tasseled Cap Transformation, to assess the extent of drought impacts. We found NBR to show the most consistent agreement with ground-based observations of drought-related tree mortality. Additionally, by integrating ground-based data from the "Dead Tree Detective" citizen science project, we were able to validate the remote sensing outcomes with a 90.22% consistency, providing confirmation of the extensive spatial distribution and severity of the inferred impacts. Our findings reveal that 13.16% of eucalypt forests and woodlands across eastern New South Wales experienced severe stress associated with drought during the 2019–2020 Black Summer drought. This study demonstrates the utility of satellite-derived drought indicators in monitoring forest health and highlights the necessity for continuous monitoring and research to understand the factors that trigger tree vitality loss.

Keywords: Drought-driven tree browning; 2019–2020 Drought; Mortality; Remote sensing; Canopy Health Score; Bioregions; Eucalypt forests and woodlands

check for updates

Academic Editor: Yihang Zhang

Received: 20 January 2025
Revised: 19 February 2025
Accepted: 27 February 2025
Published: 5 March 2025

Citation: Arampola, N.; Medlyn, B.; Hislop, S.; Choat, B.; Olin, S.; Mansourian, A.; Zhao, P.; Smith, B. Impacts of the 2019–2020 Black Summer Drought on Eastern Australian Forests. *Remote Sens.* **2025**, *17*, 910. https://doi.org/10.3390/rs17050910

Copyright: © 2025 by the authors. Licensee MDPI, Basel, Switzerland. This article is an open access article distributed under the terms and conditions of the Creative Commons Attribution (CC BY) license (https://creativecommons.org/licenses/by/4.0/).

1. Introduction

Droughts, both intensive and prolonged, are considered a global concern for forest health due to their widespread impacts on tree mortality and canopy browning [1,2]. Australia is the driest inhabited continent, with highly variable annual rainfall and frequent multiple-year intense droughts [3]. The eastern Australian climate in particular is strongly characterised by interannual variability in the El Niño Southern Oscillation (ENSO) ocean circulation pattern, with ENSO-negative phases tending to be associated with below-average rainfall, and ENSO-positive above-average rainfall over the region for periods of months up to several consecutive years [4].

As meteorological extremes such as severe droughts and heat waves become more frequent and intense [5], forests may suffer increased browning and dieback [1,6]. Tree species in the Australian landscape have evolved strategies to withstand fluctuations in precipitation and extended dry periods [3,7]. Many of the native eucalypt species are drought tolerant [8–10] and can recover through resprouting. However, recent research has highlighted a notable increase in forest mortality rates in eastern Australia, particularly evident in widespread tree browning and dieback across eastern New South Wales (NSW) in 2019 [3,11,12]. The decade spanning from 2000 to 2010 witnessed prolonged drought conditions [13], known as the Millennium Drought. A subsequent drought event unfolded from 2017 to 2019 in eucalypt forests of eastern NSW [14]. This event culminated in the summer of 2019–2020, known as the Black Summer, following the widespread and severe bushfires that occurred across much of eastern Australian, linked to the dry conditions of the vegetation and fuel loads [15]. Substantial canopy browning and mortality was observed across much of the area, peaking during the summer of 2019 and lasting until early 2020 [11]. The exceptionally dry preceding winter (June–August) and spring (September–November), coupled with overall dry conditions in 2018 despite an approximately average level of summer rainfall, contributed to this ecological impact [7]. Moreover, 2019 marked one of the hottest years on record for most of NSW [16].

It is important to understand the factors contributing to these impacts [12]. Numerous studies have investigated the factors contributing to tree browning during droughts, focusing particularly on mechanisms such as hydraulic impairment and xylem damage, carbon starvation, and increased vulnerability to pests and pathogens due to weakened defences [7,11,17–19]. Extended periods of drought can lead to water scarcity in plants, making them susceptible to stress from depleted carbohydrate reserves and reducing their resilience to co-stressors such as pests and pathogens [20,21]. The escalating frequency, intensity, and duration of droughts due to climate extremes pose a threat to the stability and growth of forest carbon sinks [12], on which emissions reduction strategies, including those in Australia, rely [22].

The lack of consistent field data on historic tree browning responses [11] leaves a gap in identifying which ecosystems across the extensive distribution of eucalypts in eastern Australia are most vulnerable to drought-induced browning or dieback, and what types of droughts, in terms of length and intensity of water deficit, can trigger this. Understanding the forest responses to drought at a larger scale and over an extended time series is essential to quantitatively assess the unusual impact compared to a long-term baseline [7]. This can be achieved through the utilisation of freely available moderate-resolution satellite remote sensing datasets [23]. Satellite-derived greenness or other similar indices offer insights into canopy responses to drought at specific time points, while analysing changes in these indices over time provides a quantitative measure of ecosystem responses to climate variability [24].

In numerous studies, the Normalized Difference Moisture Index (NDMI) [25], Normalized Burn Ratio (NBR) [11], Normalized Difference Vegetation Index (NDVI), and Tasseled Cap Transformation indices (wetness, greenness, and brightness) [26] have been identified as effective drought indicators. These indices capture spectral signal changes in vegetation due to drought stress [27], including alterations that may reflect declines in photosynthetic activity [28]. For example, [29] demonstrated that the Tasseled Cap Wetness (TCW) Index exhibits lower sensitivity to topographic variations in mature forests in the U.S Pacific Northwest. NDVI, a widely used index in ecosystem monitoring [30], serves as a proxy for various vegetation characteristics, such as greenness, productivity (i.e., estimation of absorbed photosynthetically active radiation) [31], leaf area index, and canopy water availability [32].

In contrast, NDMI is particularly sensitive to canopy moisture and has shown a strong correlation with forest growth and health decline, especially in conifer forests [33]. This sensitivity is linked to the shortwave infrared (SWIR) channel (1.55–1.75 μm), which is critical for estimating canopy water content, while the near-infrared channel accounts for variations in leaf internal structure and dry matter content. Although NBR was originally designed for fire severity assessment [34], its sensitivity to forest structure and moisture due to its use of the SWIR2 band (2.08–2.35 μm) has extended its application to general forest disturbance studies [35,36]. A comprehensive dataset derived from satellite imagery, providing high-quality outputs, can offer insights into canopy responses spectrally through spatial models [36].

A study that explored the combined effects of drought and fire impacts in *Eucalyptus* forests across forests in NSW by using Landsat long-term temporal analysis produced multiple measures for forest disturbance that allowed model validations [36]. Sentinel-2, launched in 2015, provides data with higher temporal and spatial resolution than Landsat, offering harmonization possibilities across different platforms [14,37].

Remote sensing-based models are only useful where they can be ground-truthed using observations that as far as possible cover the dimensionality and range of the model prediction space. Citizen science projects with extensive non-formal observations can help, though they need to be used with due caution. Our study takes advantage of the "Dead Tree Detective (DTD)" citizen science database, which provides ground-based information to identify areas of tree browning across much of our study domain, aiding in understanding the severity of the tree browning using photos taken by the concerned or interested public [38].

Several studies have investigated the impact of drought in Australia using global spatial indices and climatic variables [39], and others have incorporated physical parameters [12] and spectral indices at the site level [39]. Additionally, studies examining greening trends in eastern Australia have explored the effects of increasing CO_2 levels on vegetation, highlighting its potential role in modulating drought impacts [7]. These findings provide context for understanding drought impacts and inform the methods used in this study to assess ecosystem responses. While studies such as [14,40] have explored the combined impacts of drought and fire on eucalypt forests, there remains limited research specifically addressing the broader-scale impact of the Black Summer drought (2019–2020) on eastern NSW.

In this study, we present a novel approach that utilizes multiple spectral vegetation indices to investigate vegetation responses to the Black Summer drought, using harmonized dataset comprising 33 years of long-term temporal data from Landsat and Sentinel 2 images. By aligning and calibrating data from these two satellite platforms, we were able to create a consistent time series that captures vegetation dynamics over three decades. Initially, we analysed the temporal behaviour of spectral drought indicators at the site level, comparing them against a long-term baseline. Our goal was to understand the significance of the 2019–2020 drought by revealing the spectral responses of browning canopies at specific sites. Next, we extended our investigation to a broader spatial scale, examining similar browning events across a wider area. This allowed us to assess the severity and extent of the 2019–2020 drought's impact on *Eucalyptus* canopies across the region. Finally, we extracted pixels at high risk of canopy dieback or tree mortality using a threshold-based approach, which was identified from site-level responses to the 2019–2020 drought and validated using citizen science observation. Through this research, we aim to address the following questions:

1. Can satellite-derived drought indicators identify drought-induced tree mortality?

2. How significant was the 2019–2020 drought-induced tree browning in *Eucalyptus* forests in eastern New South Wales?

2. Materials and Methods

This study employs mainly two analyses: one focusing on local drought impacts at a specific site and the other examining drought across a broader spatial domain. Figure 1 provides a flowchart summarising the study's methodology. Initially, data preprocessing is conducted, which includes generating remote sensing time-series data at both the plot and regional levels. The regional-level vegetation indices time series is derived after identifying the best proxy for the field-observed drought impact data. These analyses utilize field observation data and Dead Tree Detective (DTD) data for validation. Subsequent sections detail each dataset and the specific steps involved in both the local and broader spatial analyses.

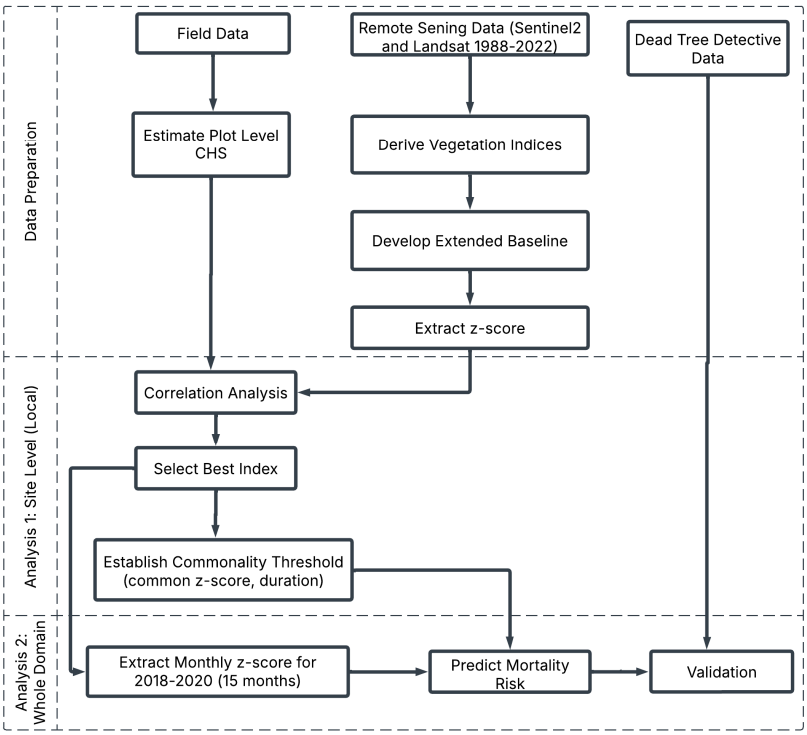


Figure 1. Flow chart of the present study.

2.1. Study Area

Our analysis covers the eastern part of the Australian state of New South Wales (NSW), between latitudes 29–37°S and longitudes 148–155°E (Figure 2a). It covers an area of ~8.75 million ha characterised by extensive areas of semi-natural forest and woodlands within a mosaic including pastoral and agricultural areas. Eucalypt-dominated forests and woodlands are a dominant feature of the Australian landscape, including in eastern NSW, where they play a critical ecological role [41]. *Eucalyptus* species are highly adapted to the Australian climate, with a range of species that can thrive in varying conditions, from the moist coastal areas to the dry inland regions [42]. The study region is characterized by diverse natural ecosystems, predominantly composed of wet and dry sclerophyll forests, dense forests, and open grasslands [43] (Figure 2b). These woodlands, characterized by an open canopy and a mix of shrubs and grasses, are dominated by species such as *Eucalyptus melliodora* (Yellow Box), *Eucalyptus blakelyi* (Blakely's Red Gum), and *Eucalyptus populnea* (Poplar Box) [44]. They function as ecological corridors, linking forest patches and providing habitats for various wildlife. The structural complexity of eucalypt forests,

with their tall, dense canopies, is crucial for the ecological balance of the region [45]. The eucalypt forests in eastern New South Wales are composed predominantly of several key species, such as *Eucalyptus pilularis* and *Eucalyptus viminalis*. These species are well-known for their adaptability to both drought and fire, which are characteristic for the ecological context in which they occur [42]. However, the increasing frequency and intensity of droughts, particularly during the 2019–20 Black Summer, have posed significant challenges to the resilience of these forests. The drought-induced stress has led to widespread canopy browning, tree mortality, and shifts in species composition, which are of particular concern for conservation and management efforts [12].

The study period is defined by the 2017–2020 drought event with the most intense meteorological variability in mid to late 2019 [46], a period characterized by severe meteorological disturbances, including drought and extensive bushfire [12,15,47]. Throughout this period, the region consistently experienced below-average rainfall, with 2019 being one of the driest years on record [11]. Figure 2c depicts this variation in rainfall for 2019, as analysed in the [16] report. The combination of extreme heat and dry conditions led to an escalation in the frequency and intensity of bushfires, particularly during the 2019–20 fire season, which saw unprecedented levels of forest destruction across NSW [48]. Field data collected at the peak of the drought (late 2019) and data from the Dead Tree Detective citizen science web portal (2019–2020) were used to assess and validate the identification of tree mortality risk areas. This process is discussed in detail in subsequent sections.

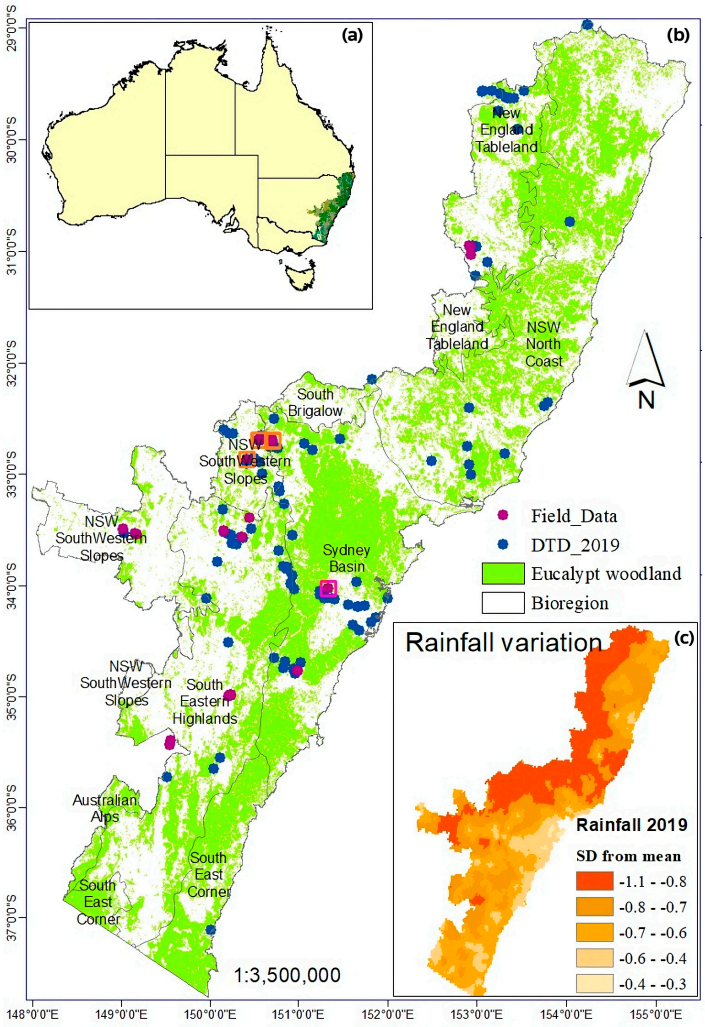


Figure 2. The study area map. (**a**) Study area location and all vegetation types according to [49] within the study area (see Supplementary File S1 (Figure S7) for details). (**b**) Study area showing *Eucalyptus*

forested areas (green) in eastern NSW, classified by the National Vegetation Information System [49]. Boundary lines indicate the bioregions, which are defined as areas with common climate, geology, and native vegetation [49]. Blue dots represent records from the Dead Tree Detective Citizen science [38] database for 2019–2020, while purple dots indicate field data collected during the drought and post-drought periods (2019–2020). The orange square box indicates the locations of the Mudgee sites, while the pink square box represents the Yellowmundee site. (**c**) The inset map shows rainfall z-score in 2019 compared to the annual average rainfall (1988–2018).

Masking Fire and Isolating Eucalypt Forest

We excluded fire-affected areas by using the Terra and Aqua combined MCD64A1 Version 6.1 Burned Area data product, which provides monthly, global gridded 500 m burned-area data from 2000 onward. Specifically, we used the 'BurnDate' layer to mask burned areas between 2004 and 2020 [48]. A dynamic and additive fire mask was applied monthly to filter out burned pixels. This mask was then applied to the Normalized Burn Ratio (NBR) calculations, derived from Sentinel-2 cloud-masked imagery, to focus on unburned vegetation. We applied a binary forest mask derived from the National Vegetation Information System [49] to isolate eucalypt forests and woodland vegetation types (Figure 2). All data processing was carried out using Google Earth Engine (GEE).

2.2. Datasets

2.2.1. Remote Sensing Data

We used both Landsat and Sentinel-2 satellite products to develop a long-term (1988–2022) time series for estimating local and spatially-extensive drought impacts in relation to a long-term baseline. Combining these two datasets enabled us to extend our analysis back in time beyond the 2015 starting point for Sentinel-2 while taking advantage of the increased resolution and more precise spectral channels of the latter instrument. The objective was to develop an extended Sentinel-2/Landsat time-series baseline, as discussed in Section 2.3.1, focusing on pixel-based monthly monitoring of 15 predetermined sites (37 plots), detailed in Section 2.2.2. These sites were selected to isolate the impact of drought, allowing us to analyse tree responses to drought on a monthly basis while preserving historical variability in each sequence [50].

Landsat data provides a long historical record useful for understanding long-term tree responses to environmental stressors [36]. We used atmospherically corrected reflectance surface data from Landsat 5 (1990–2011), Landsat 7 ETM+ (2012–2013), and Landsat 8 OLI-TIRS (2013–2022). Pixel values affected by clouds, water, and cloud shadows were omitted to ensure data accuracy. To address these gaps, we applied gap-filling methods provided by GEE (e.g., nearest neighbouring interpolation and medoid composting), which interpolate missing values using neighbouring pixel information and temporal data to maintain the continuity of the dataset [14,51]. For Sentinel-2, we used Level 1C Top-of-Atmosphere (TOA) reflectance data from 2016–2022, applying cloud masking using the QA60 cloud probability layer. Sentinel-2, with its higher temporal resolution, enabled more frequent monitoring of canopy conditions [52]. Prior research demonstrated the utility of Sentinel-2's red and SWIR bands in distinguishing healthy from stressed trees [53].

We retrieved monthly pixel data from the Landsat series (1988–2022) using the GEE platform, in order to extract site-specific data at a 30-m spatial resolution. We used the same methodology for Sentinel-2, processing data from the same sites. To ensure consistency between the two datasets, we averaged pixel values within a 30 × 30-m window and merged the nine corresponding pixels into one. To align the temporal resolutions of the both Landsat and Sentinel 2 datasets, we calculated the medoid of pixel values for each month over the entire time series (2016–2022 for Sentinel-2). The medoid, being more

robust against outliers than the mean or maximum, provided a reliable measure of typical monthly conditions ensuring a consistent and accurate time series for analysis [51].

2.2.2. Field Sites

Thresholds for canopy mortality were estimated for 15 field sites that experienced significant dieback in 2019–2020 drought. Measurements of tree health and hydraulic function at these sites during the 2019–2020 period were described by [11]. This information provided a reference point for analysing and interpreting satellite-derived metrics of vegetation stress and dieback. Importantly, these sites were not directly affected by the bush fires that occurred over parts of the study domain that same summer [11]. These 15 sites encompass a total of 37, 30 m diameter circular plots. Tree health was assessed during the 2019–2020 drought period (late 2019 and early 2020) using the visual estimation techniques established by [54] and adapted by [12]. This scoring system evaluates several crown attributes, including crown size and shape, crown foliar density, dead branches, tree epicormic growth, and leaf discoloration/browning [12]. Each attribute is scored from 0 to 5, with higher scores indicating better canopy health [11]. There were 1809 records for individual trees across all plots for the drought period measurement. For our study, we excluded all the non-*Eucalyptus* species, leaving 1397 records of individual *Eucalyptus* trees. A final Canopy health score was obtained by summing each of the constituent crown attribute scores to obtain values from 0 (dead tree) to 25 (healthy tree), similar to what was performed by [11]. We calculated basal area (BA) for each tree species in each plot. Then, we used Equation (1) to obtain an aggregated normalized Canopy Health Score within each plot (Equation (1)) [11].

$$\text{Normalized Plot Level Canopy Health Score} = \frac{\sum_{i=1}^{n}(BA_i \times CHS_i)}{\sum_{i=1}^{n}(BA_i)} \quad (1)$$

where i denotes individual tree in a plot, n the total number of trees, BA_i the Basal Area of an individual tree, and CHS_i the Canopy Health Score for the individual tree.

2.2.3. Dead Tree Detective (DTD)

Predictions of tree mortality risk (see Section 2.3.4) were ground-truthed against data from The Dead Tree Detective (DTD), a citizen-science website that documents instances of tree stress via photographs and geolocation information. This dataset contains 375 records of indication of canopy browning, tree death, or decline in vegetation health covering the 2017–2020 focus period and spatial domain of our study [38]. These records provide visual evidence of the indication of canopy browning through different photographs. We adopted a categorization system for these records that reflects the likely detectability of canopy browning from remote sensing (RS) data, rather than attempting to assign a severity score directly from the photos. For each DTD record, we inspected the NBR values for the location and time of the photograph and classified it according to whether the NBR values appeared to show browning. Based on this assessment, records were categorized into one of three classes:

Class 0: No evidence of canopy browning detectable in satellite imagery ((0)% certainty level of detectability).

Class 1: Partial evidence (detectable in approximately 50% of instances) of canopy browning in satellite imagery.

Class 2: Clear evidence (detectable in 100% of instances) of canopy browning in satellite imagery.

Records that had errors such as geo-location inaccuracies, low-quality images, or isolated reports from non-representative locations like urban backyards were not used. Non-

Eucalyptus species were also excluded. This left 118 records remaining after preprocessing, encompassing the study area.

2.3. Derivation of Vegetation Indices

Studying various VI allowed us to select the best proxy of the vegetation health in drought impacted sites. Therefore, VI such as NDVI [23,55,56], NBR [23,36,57], NDMI [23,55,58,59], Tasseled Cap Greenness (TCG) [60–62], and Tasseled Cap Wetness (TCW) [60] were selected based on their proven efficacy in detecting canopy stress and disturbances in previous studies [23]. We calculated monthly VI (see Table 1). The indices were calculated based on raw spectral and transmission band data from Sentinel-2 and Landsat missions (see Section 2.2.1).

Table 1. Summary of the vegetation indices used and their expected association with canopy browning and dieback. Where ρ is reflectance in the respective spectral bands, NIR (Near Infrared), Red, and SWIR (Shortwave Infrared) bands were utilized for calculations.

Vegetation Index	Band Combination	Link Between the Index and the Canopy Browning	Reference
Normalized Difference vegetation Index (NDVI)	$NDVI = \frac{\rho_{NIR} - \rho_{Red}}{\rho_{NIR} + \rho_{Red}}$	NDVI decreases with canopy browning, as browning reduces photosynthetic activity and green vegetation cover.	[23,55,56]
Normalized Difference Moisture Index (NDMI)	$NDMI = \frac{\rho_{NIR} - \rho_{SWIR_1}}{\rho_{NIR} + \rho_{SWIR_1}}$	NDMI decreases with canopy browning as reduced vegetation moisture content indicates stress and degradation, often leading to reduced photosynthetic activity and browning.	[23,55,58,59]
Normalized Burn Ratio (NBR)	$NBR = \frac{\rho_{NIR} - \rho_{SWIR_2}}{\rho_{NIR} + \rho_{SWIR_2}}$	NBR values decrease during drought conditions, as they reflect reduced vegetation health and soil moisture.	[23,36,57]
Tasseled Cap Greenness Index (TCG)		A decrease in Tasseled Cap Greenness reflects reduced vegetation cover and health in an area	[60–62]
Tasseled Cap Wetness Index (TCW)		Decreases in Tasseled Cap Wetness indicate reduced water content of soil and canopy moisture	[60]

We extracted the z-score of the VI considering the field plot locations and the time of observation. We considered z-scores below zero as indicators of drought disturbance, reflecting conditions where vegetation health and moisture levels were lower than the long-term average. Next, we conducted an initial analysis testing correlations between VIs and field-observed plot level CHS (See Section 3, Figure 3). This analysis identified the NBR as the most sensitive predictor of drought-induced stress. Using field-observed data from sites with known dieback, we defined a mortality risk threshold based on NBR values, which was then applied spatially across NSW to identify similar dieback events. Finally, we validated the geospatial maps generated from this analysis using the DTD database.

These steps are outlined in further detail below.

2.3.1. Developing Extended Baseline of Satellite Data

We first developed predictive relationships between Sentinel-2 and Landsat VI across sites in order to extend the Sentinel-2 backwards to create a long-term baseline. We employed a Linear Mixed Effects (LME) model, considering season as a fixed interactive effect and the site as a random effect (Equation (2)). This statistical approach is particularly

suited for handling non-independent data and for modelling the variability across different ecological data [63].

$$\text{Sentinel}_{2015–2020} \sim \text{Landsat}_{2015–2020} \times \text{Season} + \text{Random Effect by Site} \quad (2)$$

This approach allowed us to account for site-specific effects and capture the nested nature of the data, resulting in four distinct seasonal models (Table 2). Using these seasonal models, we extended the Sentinel-2 data backward from 1988 to 2022 by calibrating the Landsat data to match Sentinel-2. The predicted Sentinel-2 data, spanning from 1987 to 2015, was then fused with actual Sentinel-2 reflectance values from 2015 to 2022. This fusion technique, validated in previous studies, enhances the temporal depth of satellite-derived vegetation records, providing a continuous time series critical for long-term ecological monitoring [63,64].

Table 2. Coefficients (slope and intercept) for vegetation indices (NDVI, NBR, NDMI, TCW, TCG) derived from the Linear Mixed Effects (LME) model based on field plots. Coefficients were calculated for each season: Summer (Dec, Jan, Feb), Autumn (Mar, Apr, May), Winter (Jun, Jul, Aug), and Spring (Sep, Oct, Nov). The values R^2 represent the proportion of variance explained by the LME model for each vegetation index and season. NDVI: Normalized Difference Vegetation Index, NBR: Normalized Burn Ratio, NDMI: Normalized Difference Moisture Index, TCW: Tasseled Cap Wetness, TCG: Tasseled Cap Greenness.

Season	Vegetation Index	Slope	Intercept	R^2
Summer (Dec, Jan, Feb)	NDVI	0.611	109.25	0.66
	NBR	0.755	74.32	0.76
	NDMI	0.760	−9.91	0.74
	TCW	0.395	−641.74	0.76
	TCG	0.132	−324.32	0.75
Autumn (Mar, Apr, May)	NDVI	0.463	189.50	0.66
	NBR	0.755	74.324	0.76
	NDMI	0.692	35.98	0.74
	TCW	0.464	−431.33	0.76
	TCG	0.072	−222.68	0.75
Winter (Jun, Jul, Aug)	NDVI	0.321	266.78	0.66
	NBR	0.604	198.33	0.76
	NDMI	0.616	75.15	0.74
	TCW	0.395	−382.68	0.76
	TCG	0.054	−324.32	0.75
Spring (Sep, Oct, Nov)	NDVI	0.630	101.50	0.66
	NBR	0.732	103.50	0.76
	NDMI	0.729	18.86	0.74
	TCW	0.421	−572.24	0.76
	TCG	0.039	−209.18	0.75

To construct the continuous time series, we applied the predictive model equations (Table 2), tailored to seasonal periods based on characteristic months (e.g., December to following year's February for summer). The assumption that prediction coefficients derived

from the drought-impacted 15 site-specific plots were globally applicable across the study area was supported by the LME model's capacity to account for variability among sites.

We extended the Sentinel-2 VI data back in time over the period from 1988 to 2015 using Landsat-derived predictive coefficients (Table 2), assembling a comprehensive image stack for the study area. This stack was then merged with the actual Sentinel-2 Level 1C monthly VI dataset from 2015 to 2020, resulting in a continuous image-based time series from 1988 to 2022.

2.3.2. Extracting Z-Scores

We first calculated z-scores (see Equation (3)) for each index on a site-by-site basis, separately for the pixels overlapping each of the 37 field plots. The z score is a standardized measure that indicates how much the tree health condition, as characterised by the VI, deviates in a given month from the long-term average for that month over 1988–2022 (Equation (3)). This ensured that temporal comparisons were consistent without artificially adjusting for seasonality. Although a harmonic model could have been used to remove seasonality, as suggested by [65], the vegetative patterns in Australia are heavily influenced by dynamic rainfall events [66], which do not always follow predictable seasonal trends. This justified our methodological preference for site-specific z-score calculations.

$$\text{z-score for VI} = (\text{VI}_{\text{monthly_value}} - \text{VI}_{\text{monthly_mean}})/\text{VI}_{\text{monthly_Std}} \quad (3)$$

where VI denotes the corresponding vegetation index (Equation (3)).

The same procedure was applied to calculate z-scores for each VI across unburnt forest and woodland pixels across the entire study area.

Seasonal maps were created by compositing monthly z-score maps from 2019 to 2020 into seasons, i.e., winter = JJA, spring = SON, summer = DJF, autumn = MAM. To exclude the confounding effects of extensive bushfires that occurred across our study domain coincident with the drought effects we seek to study, we utilized fire mask images from December 2018 to February 2020 derived from MODIS global fire data at a 500 m spatial resolution [48]. For our state-wide analysis, we masked out areas that were burnt during the 2019–2020 fire season. The masking was additive: areas burned in earlier periods, such as the 2019 Spring season, remained masked in subsequent periods, including the 2019 Summer season. This cumulative masking approach ensured that all fire-affected areas were consistently excluded from our analysis across all time periods. Additive fire masks were also overlaid onto the generated z-score seasonal maps using the GEE platform. This allowed us to visually represent the spatial extent and progression of fire impacts alongside drought-induced changes in vegetation health. Further analyses were conducted in R (version 4.3.2 [67]) using RStudio.

2.3.3. Selecting Most Skilful VI for Prediction of Canopy Health Decline

To identify the satellite-derived VI most strongly associated with dieback in our field data, we plotted linear regression models and calculated a Pearson correlation matrix (Figure 3). The z-scores for each VI were extracted from the site-level time series corresponding to the dates of site inspections for Canopy Health Score (CHS) collection. After removing outliers, we retained 35 data records to analyse the relationship between the dieback metric in the field and the spectral indices. We performed linear regression using normalized variables (i.e., z-scores of VI and normalized CHS), employing the Linear Regression method from the sklearn.linear_model module in Python 3.13.1. Additionally, we assessed the strength of bivariate correlations between pairs of variables by calculating Pearson correlation coefficients, also using the scikit-learn package.

2.3.4. Identifying Mortality Thresholds

To map drought-induced dieback, we used the z-score time series for VI across the 15 study sites. The goal was to establish a commonality threshold for the period from 2019–2020 that would accurately signal the onset of drought dieback across these sites. This involved finding a combination of two parameters, a minimum z-score threshold (ZT), and an interval of duration (in months) (PT) that consistently indicated extreme drought stress.

All sites showed canopy mortality and were therefore used as a reference to test for signals of tree mortality risk. To identify a common signal across all sites, we calculated three distinct matrices based on the z-scores at our study sites.

1. Occurrence Matrix: Initially, a comprehensive matrix was developed to enumerate all possible z-score scenarios across the sites. This included examining a range of z-score thresholds from 0 to −3 and periods spanning 2 to 6 consecutive months. These z-score ranges and duration ranges were chosen by inspecting the z-score time series derived from a long baseline for each site individually (Figure 4). For instance, a condition such as a z-score below −1 for three consecutive months was assigned a count of 1. We then aggregated the number of sites meeting these conditions, calculating the proportion of sites that satisfied each specific criterion out of the total number of sites, and we took the percentage. This matrix provided a quantitative basis for identifying common thresholds that indicate significant drought impact across the site for the period from 2019–2020.
2. Severity Matrix: Subsequently, a severity matrix was constructed to quantify the cumulative impact of remaining below a certain z-score threshold for a designated period. This matrix aimed to capture the prolonged severity of drought conditions across the sites.
3. Product Matrix: The final step involved creating a product matrix that integrated the severity of drought conditions with their occurrence across the study sites. By combining the likelihood and severity metrics for drought impacts, this step facilitates the identification of critical thresholds for mortality risk.

The lowest values along the diagonal of the product matrix thus corresponded to the most severe and chronic drought conditions across the field sites. The range of lowest values exhibited different percentages of occurrence. Based on occurrences approximately equal to 90%, 75%, 50%, and 25%, the corresponding z-scores and durations in months were extracted. These percentages were then used to define different levels of drought impact (Table 3). This approach allowed us to identify z-score thresholds for each VI that corresponded to varying levels of drought severity and their associated mortality risks.

Table 3. Classification of drought impact levels based on percentage of occurrence across field sites. The approximate z-scores and corresponding time in months are associated with each percentage of occurrence. Higher percentages reflect more widespread occurrences of the given level of impact across the 37 field study plots.

Percentage of Occurrence Across Sites	The Level of Drought Impact	The Minimum Threshold for z-Score (ZT)	The Duration of Consistency of z Score (in Months-PT)	Threshold Number
90%	Moderate browning for moderate period	−0.75	3	Threshold_1
75%	Moderate browning for extensive period	−1.5	2	Threshold_2
50%	High browning for moderate period	−1.75	2	Threshold_3
25%	High browning for extensive period	−1.75	4	Threshold_4

2.3.5. Scaling up Mortality Risk Across Study Area

We applied the z-score and duration thresholds pixel by pixel to the remotely sensed data across NSW through time to produce a detailed drought severity map highlighting

the different impact scenarios depicted in Table 3. The inputs for the analysis included a stack of z-score NBR images captured monthly from the summer of 2018 to the summer of 2019 (15 months in total) and predefined thresholds (ZT, PT). For each time period (PT), we stacked z-score maps and applied the corresponding ZT threshold to identify pixels with values below the threshold. This created a binary matrix (true/false) to indicate exceedence of the threshold. Pixels that met the criteria for all time periods were retained for further analysis. For each of these pixels, the minimum z-score value across the considered time periods was selected. This process was repeated iteratively for all time steps in the z-score image stack. The minimum z-score values for each pixel were aggregated into a final image, representing the overall minimum values across the entire period. This process could identify pixels that meet multiple thresholds (e.g., a pixel satisfying Threshold_1 could also meet the criteria for Threshold_2). To resolve this, we assigned each pixel to the highest threshold that it met, e.g., if a pixel met both Threshold 1 and 2, it was assigned to Threshold 2. This stratified approach enabled us to spatially visualize the most extreme drought impacts across the study area. By applying the thresholds over both time and space, we were able to identify regions that experienced significant drought severity during the 2019–2020 drought event. To quantify the spatial extent of a given severity level, we calculated the fraction of affected area relative to the total *Eucalyptus* forest and woodland across the study site for each threshold separately.

This method provided a framework for detecting and mapping drought vulnerability across our study domain. It also allowed us to identify severely impacted areas, suitable for closer analysis to understand the ecological consequences of prolonged drought conditions.

2.3.6. Validating Predicted Mortality Risk

To ensure the threshold maps accurately depicted the extent of extreme drought events across NSW for 2019–2020, we implemented a visual-based validation process using the 118 records covering 2019–2020 from the DTD dataset.

The four threshold maps (see Section 2.3.5) were overlaid in a hierarchical manner (from Threshold_4 to Threshold_1). We then overlaid the filtered DTD points onto the threshold maps (Figure S6). These DTD records vary in their certainty regarding the detection of mortality signals at different spatial scales. Since the DTD record locations do not necessarily represent the exact centres of forests or woodlands and the threshold pixel in the map, we applied a 1 km x 1 km buffer around each geolocation, assuming this buffer would encompass a representative patch of woodland area. This buffer was then used to capture the threshold pixels enclosed within the buffer zone of corresponding DTD record on the severity map of z-scores, which were derived specifically for *Eucalyptus* forests within the study area. To determine how many mortality risk pixels were captured by each buffered DTD record, we used the zonal statistics tool in QGIS. This tool calculates statistics for a raster layer based on the features of an overlapping polygon vector layer. Specifically, we calculated the count of mortality pixels within each buffer zone. We then applied a condition to each DTD location individually: if the count of mortality pixels within the buffer zone was greater than 0, we considered the DTD record to have detected a mortality risk; otherwise not. Here, we assumed that a single pixel, representing a 30×30 m^2 ground area, constitutes a considerable spatial extent of mortality risk. Therefore, if at least one pixel within the buffer zone meets the criteria for any threshold number, it is sufficient to classify the corresponding DTD record as having detected mortality risk. We then calculated the number of DTD records for each category of mortality detection certainty that satisfied the condition and tabulated the results. The percentage of total DTD records capturing canopy browning, which may indicate canopy dieback and potentially reflect tree mortality risk, was calculated to estimate how well different levels of DTD points

detected dieback risk. This detectability was further assessed using comparisons between the threshold class and the photograph from the DTD record (see Supplementary File S2).

3. Results

Following the correlation analysis between the various z-scores of the VI and CHS of field sites, we determined that z-scores derived from the NBR performed optimally as indicators for drought-induced tree browning across 15 sites. The results presented here are based on the NBR index.

3.1. Comparison of VI Z-Scores with Field Observations

Figure 3 illustrates the correlation between each VI and CHS, extracted over the same time, i.e., the 2019–2020 drought, across 15 sites. Among the VI candidates examined, the z-score of the NBR exhibited the highest |R| value, indicating a moderate correlation with field-observed CHS (Figure 3a). Pearson correlation coefficients likewise show NBR to be the best predictor (Figure 3f). NDVI, NDMI, and TCG demonstrated a particularly weak relationship across the sites. Overall, although the sites across the different bioregions exhibited high variability, with no clear clustering pattern, NBR was selected as the best at predicting canopy mortality (Figure 3a–e). Further results presented are all based on NBR.

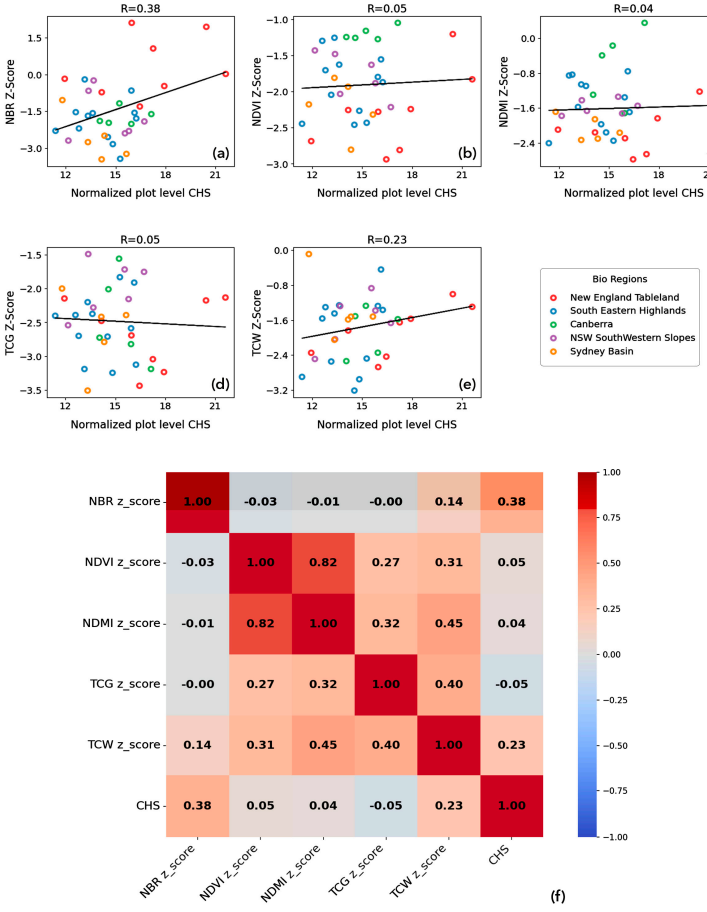


Figure 3. Regression plots for the 15 field sites (37 plots) during the 2019–20 drought showing the relationship between satellite-derived drought indicators (z-scores) and normalized plot canopy health scores (CHS) across different bioregions. (**a**–**e**) Correlation between the vegetation indices namely, normalized burn ratio, normalized difference vegetation index, normalized difference moisture index, tasseled cap greenness, and tasseled cap wetness index and the field observation canopy health score data. The |R| for each correlation is shown in the top of the graph, and (**f**) shows the Pearson correlation coefficients of VI and field observation.

3.2. Temporal Variation of Drought Impacted Sites

Seasonal variation can be observed across the whole time series in both the selected sites; normally, the summer periods (December–February) have a lower value while the winter periods (June–August) have a higher value (Figure 4a,c). There is also significant interannual variability. For instance, there was a decline in NBR and z-scores from 2006 to 2008, followed by a typically higher NBR and positive z-scores from 2008 to 2013, as shown in (Figures 4a and S1). Most of the field sites exhibited a similar trend (Figure S1), with sites in the Southeastern Highland (SEH) bioregion typically showing significantly lower NBR levels during 2019, where z-scores were lower than −2 for prolonged periods (more than six months). A significant drop in z-scores, lower than −1.5, consistent over more than four months, was observed during 2019–2020, except at the Yellowmundee site (Figure 4a,c). During the drought peak years of 2019–2020, Figure 4b,d illustrates a significant deviation between the NBR values and their long-term monthly baseline and standard deviation starting in mid-2019. At the peak of the drought (i.e., summer 2019–2020), most of the field sites regardless of bioregion showed an extremely low z-score, with most of the sites showing values lower than −1 for more than 3 months consistently (Figures 4 and S1–S5).

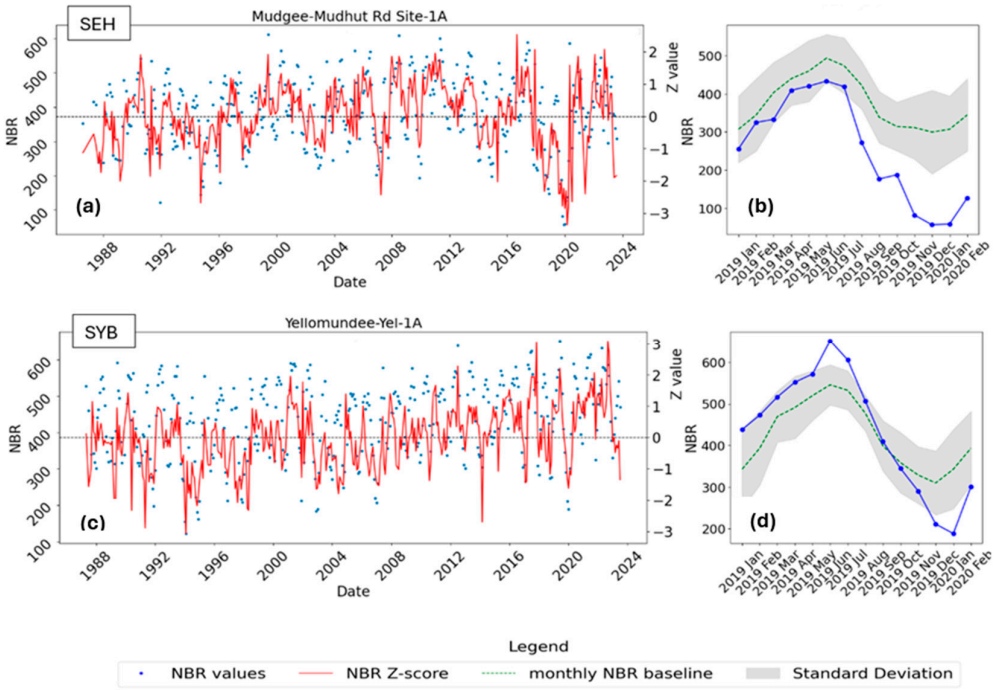


Figure 4. Time series of the monthly NBR and z-scores at two example sites, Mudgee (Southeastern Highlands bioregion) and Yellowmundee (Sydney Basin bioregion) (see Figure 2). (**a**–**c**) The long-term monthly Sentinel-2 time series from 1988 to 2022. Blue dots represent the harmonized NBR values from Landsat (1988 to 2015) and actual Sentinel-2 NBR raw values from 2015 to 2022, which aggregate for 30 m spatial resolution. The red line represents the z-scores derived from monthly NBR values, ranging from −3 to +3 on the right-hand side axis. (**b**–**d**) A close-up of the 2019 Black Summer drought event, showing the long-term monthly mean (green dashed line), the monthly NBR values for the period of 2019–2020 (blue line connected with dots), and standard deviations (grey shaded area).

3.3. Spatial Pattern of Drought Impact Across the Study Area

Maps of the NBR z-scores (Figure 5) reveal a clear spatial pattern of vegetation condition, with the most severe drought impacts (indicated by brown, red, and orange zones) concentrated in the southern and central bioregions, including the Southeastern Slopes (NSS), Southeastern Highlands (SEH), New England Tableland (NET), and Australian Alps

(AA). The greatest impact of drought was observed during Summer 2019–2020, where extensive areas showed significantly negative NBR z-scores (Figure 5).

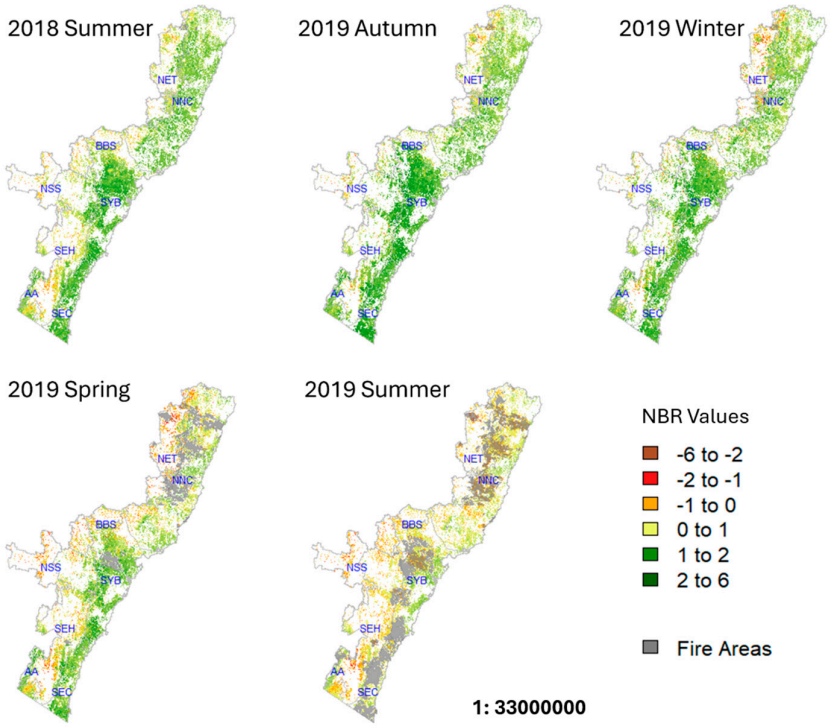


Figure 5. Seasonal time-series maps of NBR z-scores (30 m resolution) for the *Eucalyptus* Forest in eastern NSW during the peak of the 2019–2020 drought period. Areas masked for fire are displayed in grey. White areas are the non- *Eucalyptus* areas. The abbreviation of the bioregions are NET: New England Tableland, NNC: NSW North Coast, BBS: South Brigalow, SYB: Sydney Basin, NSS: NSW Southwestern Slopes, SEH: Southeastern Highlands, AA: Australian Alps, SEC: South East Corner.

Between Summer 2018 and Autumn 2019, there was a noticeable improvement in vegetation health (represented by green areas), particularly in northern bioregions such as NET and NNC (Figure 5). However, Winter 2019 saw a recurrence of browning, especially in the northeastern regions (Figure 5). The overlay of fire-affected areas highlights a strong alignment with regions of severe impact, particularly in the southern bioregions (SEH, AA) during Summer 2019 (Figure 5). In the southeastern corner and Sydney Basin bioregions, significant drought impacts were evident during Spring 2019 and Summer 2019 (Figure 5). Conversely, northeastern bioregions experienced a gradual increase in drought severity throughout the entire period and were severely impacted by extensive bushfires in 2019. Extreme drought effects were most pronounced in the southern part of the North Coast, Southern Highlands, Southwestern Slopes, and parts of the South Brigalow bioregions, with Summer 2019–2020 exhibiting the most severe tree browning compared to other seasons.

3.4. Categorisation of Drought Severity and Mortality Risk

Figure 6 illustrates the spatial variability in drought impact on *Eucalyptus* forests and woodlands across the study area, showing that the effects were not uniform. Some regions experienced more severe and prolonged impacts than others. High levels of browning were particularly visible in the northwestern, inland, and southwestern areas (Figure 6). In the northern bioregions into the west direction, including the NSW North Coast and New England Tableland, pixels with z-scores lower than −1.75 for a consistency of two months (Threshold 3) and 4 months (Threshold 4) were observed (Figure 6, Table 4). These areas represent approximately 8.30% of the total *Eucalyptus* forest area (Table 4). Pixels

with z-scores below −1.75 for four months (Threshold 4) were concentrated in the New England Tablelands and Southeastern Highlands bioregions (Figure 6, Table 4). These areas account for 5.34% of the total *Eucalyptus* woodlands (Table 5). Moderate browning was more widespread in the southern and central parts of the study area (Figure 6). Moderate browning accounted for 4.86% of the *Eucalyptus* forest area (Table 4). Notably, the southeastern corner and the Sydney Basin showed significant mortality pixels over both moderate and extended periods. In total, 13.16% of the *Eucalyptus* forests were impacted by the 2019–2020 drought (Table 4).

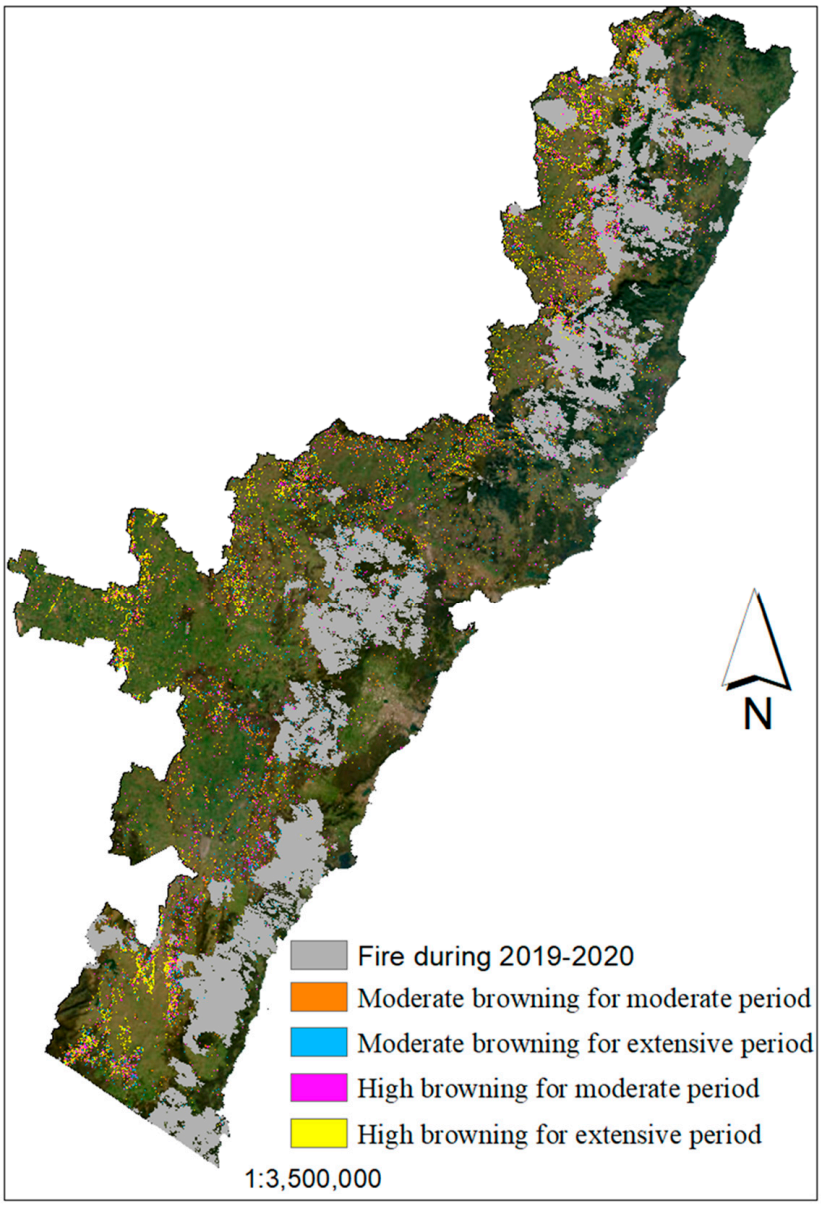


Figure 6. Drought-induced tree browning categorised by intensity and duration of impact across eucalypt forest and woodlands of the study area (see Table 3). This map shows affected pixels categorized into four severity levels based on two parameters: z-score-based thresholds, and the consistency period during which the z-scores were retained.

Table 4. The percentage of drought-affected areas as a fraction of the total *Eucalyptus* forest across the study area. The total number of pixels representing *Eucalyptus* forest and woodlands, resampled to a 30 m resolution, is 97,233,706.

Threshold Category	Threshold Value		Number of Pixels	Damaged Woodland Area (Mha)	Drought-Impacted Area as a Fraction of Total *Eucalyptus* Forest (%)
	(Z_T)	(P_T)			
Moderate browning for moderate period (Threshold_1)	−0.75	3	2,593,456	0.233	2.67
Moderate browning for extensive period (Threshold_2)	−1.5	2	2,134,971	0.192	2.19
High browning for moderate period (Threshold_3)	−1.75	2	2,877,745	0.259	2.96
High browning for extensive period (Threshold_4)	−1.75	4	5,187,233	0.467	5.34
Total	-		12,793,405	1.151	13.16%

These areas account for 5.34% of the total *Eucalyptus* woodlands (Table 4). Moderate browning was more widespread in the southern and central parts of the study area (Figure 6). Moderate browning accounted for 4.86% of the *Eucalyptus* forest area (Table 4). Notably, the southeastern corner and the Sydney Basin showed significant mortality pixels over both moderate and extended periods. In total, 13.16% of the *Eucalyptus* forests were impacted by the 2019–2020 drought (Table 4).

3.5. Validation of Predicted Mortality Risk

Table 5 summarizes how many DTD records coincide with pixels deemed to be under a mortality risk. Out of the nine DTD records deemed unlikely to show mortality risk in satellite imagery, four nonetheless overlapped with pixels classified as having some level of mortality risk (i.e., 3.39% as a percentage). However, five records did not correspond to any detected mortality risk classification (Table 5). Out of the 28 records classified under the 50% certainty level of capturing the mortality risk, 23 records (82.14%) coincided with pixel regions identified as being under a mortality risk. There were 81 points classified with 100% certainty in their ability to capture browning canopy patches through satellite data, fully aligning with regions identified as being under a mortality risk by the NBR-based classification. This indicates that more than 68% of DTD records successfully identified mortality risk pixels. Overall, 108 out of the 118 DTD records were consistent with the NBR-based classifications, resulting in an agreement rate of 91.52% across the entire study area. The DTD points with mortality detection capability were then visually assessed.

Table 5. The summary of the agreement between DTD records of drought-related tree canopy loss with pixels identified as being at mortality risk across the study area. User accuracy refers to the percentage of correctly identified mortality risk records relative to the total number of records in the DTD dataset.

Category of DTD	Certainty Level of Capturing Remote Sensing (RS) Mortality Data	Total Number of DTD Records in the Category	Number of Records That Coincide with Pixels Deemed at Mortality Risk	The Percentage of Points That Coincide with Pixels Deemed at Mortality Risk (%)	User Accuracy (%)
0	0%	9	4	44.45	3.39
1	50%	28	23	82.14	19.49
2	100%	81	81	100	68.64
Total		118	108	91.52	91.52

Figure 7 shows examples of DTD photo-based records and the corresponding mode of the threshold category (i.e., browning level of the mortality matrix) (Figure 7 and Table S1). Prolonged periods of high stress conditions were visually confirmed to show high levels of

browning impact over larger areas, while moderate browning over shorter periods resulted in less impact over smaller areas (Figure 7). The colour change from green to brown was less pronounced in areas with moderate browning over moderate periods (Figure 7). Considering the seven selected sample locations (see Figure S6) used to cross-check severity levels with photo-based data, we found that regardless of the severity level detected from the remotely sensed threshold map, all levels exhibited a significant degree of tree browning in the DTD photos.

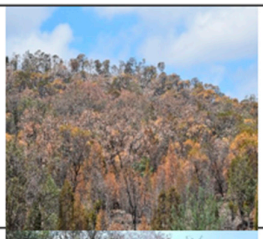
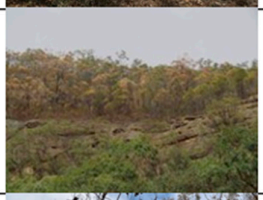
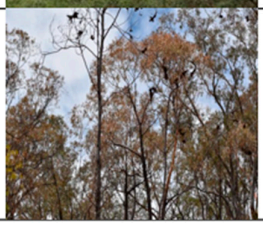
Severity level of mortality	Evidence taken from DTD records
High browning for extensive period	
High browning for moderate period	
Moderate browning for extensive period	
Moderate browning for moderate period	

Figure 7. Examples of browning levels visualized in the DTD for a sample of records overlaid on the mortality threshold map.

4. Discussion

Our results confirmed that it is feasible to identify drought-induced tree canopy dieback over extensive regions using moderate-resolution satellite sensors, such as those onboard the Sentinel-2. Among the five selected potential vegetation indices (VIs), we found that the Normalized Burn Ratio (NBR) was associated best with observed dieback at our field sites, although the association was relatively weak. Limitations in satellite resolution or variability in field observations may have contributed to the weaker correlation [68]. A relatively weak association is expected because certain attributes of the CHS, such as canopy size and epicormic growth, may not produce consistent spectral signals capable of being captured by spectral indices such as the ones that were tested. This relationship between spectral responses and field-observed dieback enabled us to develop a method for identifying dieback events across our eastern Australian study region. Association using visually reported citizen science data showed a satisfactory agreement between predicted mortality risk based on the size and duration of negative NBR anomalies and reported local canopy loss. Our threshold-based approach to account for both the severity and duration of

the drought impacts indicated that the severe drought culminating in the 2019–20 summer impacted 13.16% (1.151 Mha) of *Eucalyptus* forests and woodlands across our study region.

Our study shows that spectral indices from different wavelength ranges correlate variably with severe drought impacts across diverse eucalyptus bioregions. While indices based on red, green, blue, and near-infrared wavelengths (e.g., NDVI, Tasseled Cap Greenness and wetness) capture overall vegetation greenness and canopy moisture, they are less sensitive to the subtle declines in leaf water content and structural degradation that occur during severe drought [23]. In contrast, indices that incorporate shortwave infrared wavelengths NDMI (using SWIR1: ~1.55–1.75 μm), NBR (using SWIR2: ~2.08–2.35 μm), and Tassled Cap Wetness better capture variations in canopy water content and structural integrity [25]. However, [25] demonstrated that NDMI provided better spectral separability for drought disturbance than TCW due to lower omission errors. Additionally, [23] provided significant evidence ($\alpha < 0.05$) showing a strong correlation between NDWI and species-level tree mortality assessments, suggesting that the red and NIR wavelengths are less effective at capturing water content variations compared to the SWIR bands. Since leaf water content and photosynthetic pigment abundance both influence reflectance in the visible spectrum [69], drought stress monitoring should prioritize the 1300–2500 nm spectral region where reflectance is primarily affected by leaf water content [70]. Notably, Ref. [11] demonstrated that NBR effectively detects canopy browning in drought-impacted areas with significant mortality (e.g., >37% basal area dead), a finding that aligns with our results and suggests that the SWIR2 band in NBR is more sensitive to severe water loss and structural changes than the SWIR1 band used in NDMI. This supports our findings, suggesting that NBR is a stable indicator for assessing drought-induced tree mortality across heterogeneous landscapes.

The observed differences between index performance and stressed tree observations may also be attributed to site heterogeneity. Variations in vegetation types, canopy density, and topography influence signal penetration and reflectance from forest canopies [14,46], potentially affecting the relationship between spectral indices and observed drought impacts [14]. For example, dense canopies can restrict electromagnetic signal penetration to only the uppermost leaves, whereas sparse canopies may allow greater interaction with understory vegetation or the soil background [7]. Our findings reveal significant temporal and spatial variability in drought-induced tree browning across different locations in NSW, during the drought peak period. This aligns with previous research, such as [11], who also identified the NBR as a reliable indicator of vegetation stress, particularly in response to drought. The decline in tree cover in this region was observed to have begun as early as 2017, with visible stress symptoms appearing prior to the 2019–2020 fires [7].

The long-term time-series analysis of eastern NSW revealed significant drought-induced tree browning, marked by notable declines in z-scores (below −1 during later month of 2019) across both spatial and temporal scales when the drought was at its peak. z-scores offer a standardized measure of forest health, valuable for comparisons across species, regions, and potentially seasons, facilitating monitoring over time and across diverse landscapes [68]. Furthermore, integrating multiple indices and environmental factors through redundancy analysis has been shown to improve the accuracy of forest health assessments, as demonstrated by [39].

The use of spectral-based browning metrics, specifically the monthly NBR z-score from a long-term baseline, effectively identified drought-induced dieback in eucalypt forests, capturing even subtle changes in canopy health. A study [68] conducted in Sierra Nevada forests in the western USA supports our findings, demonstrating that remote sensing indices based on long-term baselines were able to accurately classify 96.3% of actual tree mortality areas using monthly time-series data. Although [14] demonstrated the utility

of dense Sentinel-2 time series data for monitoring forest disturbances, including those from fire and drought in the same region, their study identified drought impacts over approximately 4.1 Mha (i.e., 20.5% of eucalypt forest damage), which is more than three times the area identified in our study. This discrepancy may be attributed to their use of a shorter pre-event stable period, necessitated by the limited availability of Sentinel-2 data. Our study was able to overcome this limitation by integrating historical data from Landsat to construct a 33-year time series, from which the monthly average was used as the baseline. Establishing a long-term baseline is crucial for assessing forest health, as it enables the effective quantification of drought impacts [68].

Spatially, regional climate, soil properties, and local ecosystem dynamics play crucial roles in shaping responses to drought, leading to varied tree mortality patterns across landscapes. Many *Eucalyptus* species experienced severe hydraulic stress, with leaf water potential dropping significantly, although some species displayed resilience, particularly those in semi-arid regions [71]. More arid settings were found to have higher drought sensitivity for canopy properties but lower sensitivity to biomass loss, as reported by [24].

However, a NBR time series analysis from 2017–2019 across NSW conducted by [11] demonstrated a similar decline during the peak of the drought, suggesting a severe reduction in NBR compared to previous droughts. While significant tree mortality was observed during the Millennium Drought, the lack of consistent forest monitoring posed challenges in quantifying the impact. Studies indicate that the 2019–2020 drought may have resulted in more substantial tree mortality than the Millennium Drought [3]. The 2019–2020 drought was notable for its widespread vegetation decline and mortality, with nearly 50% of forest areas falling below disturbance thresholds [14]. Structural changes, such as increased stem density and reduced canopy height, observed by [72], indicated low resistance and resilience to severe drought events. The challenges in predicting ecological responses, due to the limited understanding of the direct and indirect effects of environmental changes, were highlighted by [73]. Tree dieback is often triggered when critical drought stress thresholds are crossed, rather than by a gradual increase in stress, as discussed by [74]. This understanding is also supported by evidence from [1,75,76], who emphasize the non-linear nature of the drought-dieback relationship.

Our study was able to provide evidence that anecdotal evidence and visual reports, such as those from the Dead Tree Detective project, can be valuable tools for understanding the impact of drought in Australia [3,77]. Visually inspecting drought-induced tree death records and comparing them to remotely sensed data proved effective, with 88.13% of identified high-mortality-risk pixels aligning with DTD records. This approach offers valuable insights, particularly in studies where severe DTD impacts are observed but are difficult to correlate with remote sensing measurements. For instance, [3] found that hydraulic model predictions of tree mortality during the severe 2019–2020 drought in Eastern Australia did not align with remote sensing observations, despite photographic evidence of tree decline in DTD records, albeit with uncertainty regarding the cause. Our study attempted to address this gap by collecting more comprehensive data on vegetation decline during drought citizen science efforts.

Varying levels of severity across heterogeneous environmental conditions may be due to the unique adaptations that *Eucalyptus* species in each bioregion have evolved [74,78]. The high level of severity observed in northern and western regions may suggest that *Eucalyptus* forests in these areas are more prone to drought-induced tree stress compared to other regions. Other studies have shown a correlation between tree size and canopy dieback due to hydraulic failure during extreme drought events [12], while [72] highlighted susceptibility among Mediterranean-type forests under similar conditions. Drought impacts are often greatest when pronounced water deficits are sustained for a prolonged

period. A study conducted in central European floodplain forests during very dry years in 2018–2019 identified significant threats posed by consecutive extreme heat and drought to forests, even those that were typically well-watered [79]. Climate change is likely to lead to more frequent and severe droughts, exceeding trees' resistance to such extreme conditions, and resulting in more widespread and sudden dieback events, as suggested by [72]. Tree mortality during recent droughts was even more severe than during the Millennium Drought from 2000 to 2009 [3]. Reflecting on a previous analysis [11], we conclude that severe drought has a profound effect on tree health, potentially through impacts on hydraulic function and subsequent canopy dieback, in extreme cases leading to tree mortality [3,11,14].

Limitations of the Current Study

One key limitation of this study is the lack of field data on tree health before, during, and after the drought event, limiting our ability to fully assess the temporal sequence of impacts ultimately resulting in tree vitality loss, as well as possible recovery once rains return (as they did in February 2020 in our study area). Additionally, the relatively small number of field sites for which direct observations of canopy condition were available to inform our study potentially limited the prediction skill of our model and the spatial representativeness of our findings. The development of continuous, long-term, and spatially extensive field monitoring of drought affected forests and woodlands would enable more powerful future studies that improve predictability and enable richer mechanistic insights from future studies using similar methods.

The validation of the NBR-based mortality risk classification using the DTD dataset presents several limitations. The validation process is partly circular. Because the DTD dataset was stratified according to whether canopy browning was detectable in satellite imagery, these same satellite observations are then used to 'validate' the NBR-based classification. While this approach leverages the best available data, it does not represent a fully independent assessment of remote-sensing outputs. Additionally, the quality and consistency of DTD photographs vary significantly, making it difficult to assign precise severity levels directly from the images on the canopy browning levels. Many photographs were taken horizontally or focus on trunks and branches, rather than providing clear canopy-level perspectives. Despite these constraints, using DTD records for validation provides a valuable, if partial, means of corroborating the remotely sensed detection of tree mortality risk.

Our study relied solely on optical, moderate-resolution satellites (Landsat and Sentinel-2). Future research could integrate sensors, such as radar and LiDAR, or use data fusion techniques combining optical and radar imagery, which potentially detect or correlate with other aspects of canopy condition and response, not directly detectable using optical reflectance data, such as leaf or stem water content [80]. This approach could potentially provide a more comprehensive understanding of tree responses and vulnerabilities to extreme events like drought, adding to insights from optical approaches, as deployed in this study.

The severity of drought-induced browning effects varies depending on the duration and intensity of the drought, and is influenced by landscape factors such as climatic, geographical, and topographical factors, as well as the local vegetation type. Previous studies have shown that vegetation vulnerability to stress can be affected by general productivity, including the fertilization effect of CO_2 and soil nutrient status as well as soil water. Our study could be extended by incorporating an analysis of environmental and landscape factors that interact with the canopy condition. The causes of drought-induced tree mortality have complex relationships with the aforementioned factors. Machine

learning and deep learning approaches, such as Long Short-Term Memory (LSTM), could be ideal for understanding the underlying factors of drought mortality.

While our research focused on identifying the impacts of drought, we did not investigate the processes of drought recovery. Future studies should explore the factors that influence vegetation recovery following drought events, as this could provide further insights into the resilience of different ecosystems and help refine predictive models for future drought scenarios. Field campaign recovery data did not show a consistent relationship with spectral reflectance from satellite data, highlighting the challenges in studying tree recovery post-drought, as noted by [11]. Future studies should consider deep learning approaches to identify the factors behind the recovery process of drought-impacted trees.

5. Conclusions

Our analysis revealed that the 2019–20 drought was significant compared to the long-term temporal baseline. Additionally, the Normalized Burn Ratio (NBR) index was confirmed as a good indicator for capturing drought-impacted signals in eucalypt forests over a wide spatial scale.

The poor correlation and high variability between field data on tree health and satellite-derived drought mortality metrics may be due to inherent differences between bioregions. To improve accuracy in assessing canopy health from satellite data and identifying the causes of drought-induced tree mortality, additional environmental factors should be considered. Future studies should focus on different bioregional environmental factors contributing to drought-related tree mortality. The use of machine learning and deep learning algorithms to explore complex relationships between tree mortality and contributing factors may be useful to provide nuanced insights into the underlying causes of tree mortality.

Supplementary Materials: The following supporting information can be downloaded at: https://www.mdpi.com/article/10.3390/rs17050910/s1, in Supplementary File S1, Figure S1 to Figure S5: Time series of the monthly vegetation indices and z-scores at all the sites across the study area. In Supplementary File S2, you can find Figure S6: Drought-induced tree browning areas as a fraction of the total Eucalyptus forests and woodlands, overlaid with DTD locations; Figure S7: Different vegetation types exist across the entire study area, according to the classification based on National Vegetation Information System Version 6.0; and Table S1: Examples of photo instances from the DTD (Dead Tree Detective web portal) for different geographic locations across the study area.

Author Contributions: Conceptualization, N.A., B.S., B.M., S.H., B.C., S.O., A.M. and P.Z.; methodology, N.A., B.S., B.M., S.H., B.C. and S.O.; software, N.A., S.H. and B.M.; validation, N.A., B.S., B.M., S.H., B.C. and S.O.; formal analysis, N.A., B.S., B.M., S.H., B.C., S.O., A.M. and P.Z.; investigation, N.A., B.S., B.M., S.H., S.O. and A.M.; resources, B.S.; data curation, B.C.; writing—original draft preparation, N.A.; writing—review and editing, N.A., B.S., B.M., S.H., B.C., S.O., A.M. and P.Z.; methodology, N.A., B.S., B.M., S.H., B.C. and S.O.; visualization, N.A.; supervision, B.S. All authors have read and agreed to the published version of the manuscript.

Funding: This research was funded in part by the Lund University Strategic Research Area Modelling the Regional and Global Earth System (MERGE), funded by the Swedish Government.

Data Availability Statement: Dataset available on request from the authors.

Acknowledgments: The authors acknowledge the financial support provided to N.A through the Australian Government Research Training Program Scholarship, which enabled the undertaking of this research. The Commonwealth's contribution is gratefully acknowledged, as it played a vital role in facilitating this research project. The findings and outputs presented in this work reflect the research efforts undertaken as part of the Research Training Program Scholarship. We thank three anonymous reviewers for valuable comments that led to improvements in the paper.

Conflicts of Interest: The authors declare no conflicts of interest. The funders had no role in the design of the study; in the collection, analyses, or interpretation of data; in the writing of the manuscript; or in the decision to publish the results.

References

1. Allen, C.D.; Macalady, A.K.; Chenchouni, H.; Bachelet, D.; McDowell, N.; Vennetier, M.; Kitzberger, T.; Rigling, A.; Breshears, D.D.; Hogg, E.T.; et al. A global overview of drought and heat-induced tree mortality reveals emerging climate change risks for forests. *For. Ecol. Manag.* **2010**, *259*, 660–684. [CrossRef]
2. Allen, C.D.; Breshears, D.D.; McDowell, N.G. On underestimation of global vulnerability to tree mortality and forest die-off from hotter drought in the Anthropocene. *Ecosphere* **2015**, *6*, art129. [CrossRef]
3. De Kauwe, M.G.; Medlyn, B.E.; Ukkola, A.M.; Mu, M.; Sabot, M.E.B.; Pitman, A.J.; Meir, P.; Cernusak, L.A.; Rifai, S.W.; Choat, B.; et al. Identifying areas at risk of drought-induced tree mortality across South-Eastern Australia. *Glob. Change Biol.* **2020**, *26*, 5716–5733. [CrossRef] [PubMed]
4. Teckentrup, L.; De Kauwe, M.G.; Pitman, A.J.; Smith, B. Examining the sensitivity of the terrestrial carbon cycle to the expression of El Niño. *Biogeosciences* **2021**, *18*, 2181–2203. [CrossRef]
5. Mitchell, P.J.; O'Grady, A.P.; Hayes, K.R.; Pinkard, E.A. Exposure of trees to drought-induced die-off is defined by a common climatic threshold across different vegetation types. *Ecol. Evol.* **2014**, *4*, 1088–1101. [CrossRef]
6. Fettig, C.J.; Mortenson, L.A.; Bulaon, B.M.; Foulk, P.B. Tree mortality following drought in the central and southern Sierra Nevada, California, U.S. *For. Ecol. Manag.* **2019**, *432*, 164–178. [CrossRef]
7. Rifai, S.W.; De Kauwe, M.G.; Ukkola, A.M.; Cernusak, L.A.; Meir, P.; Medlyn, B.E.; Pitman, A.J. Thirty-eight years of CO_2 fertilization has outpaced growing aridity to drive greening of Australian woody ecosystems. *Biogeosciences* **2022**, *19*, 491–515. [CrossRef]
8. White, D.A.; Beadle, C.L.; Worledge, D. Leaf water relations of *Eucalyptus globulus* ssp. globulus and *E. nitens*: Seasonal, drought and species effects. *Tree Physiol.* **1996**, *16*, 469–476. [CrossRef]
9. Bourne, A.E.; Creek, D.; Peters, J.M.; Ellsworth, D.S.; Choat, B. Species climate range influences hydraulic and stomatal traits in Eucalyptus species. *Ann. Bot.* **2017**, *120*, 123–133. [CrossRef]
10. Li, X.; Blackman, C.J.; Choat, B.; Duursma, R.A.; Rymer, P.D.; Medlyn, B.E.; Tissue, D.T. Tree hydraulic traits are coordinated and strongly linked to climate-of-origin across a rainfall gradient. *Plant Cell Environ.* **2018**, *41*, 646–660. [CrossRef]
11. Losso, A.; Challis, A.; Gauthey, A.; Nolan, R.H.; Hislop, S.; Roff, A.; Boer, M.M.; Jiang, M.; Medlyn, B.E.; Choat, B. Canopy dieback and recovery in Australian native forests following extreme drought. *Sci. Rep.* **2022**, *12*, 21608. [CrossRef] [PubMed]
12. Nolan, R.H.; Gauthey, A.; Losso, A.; Medlyn, B.E.; Smith, R.; Chhajed, S.S.; Fuller, K.; Song, M.; Li, X.; Beaumont, L.J.; et al. Hydraulic Failure and Tree Size Linked with Canopy Die-Back in Eucalypt Forest During Extreme Drought. 2021. Available online: https://onlinelibrary.wiley.com/doi/10.1111/nph.17298 (accessed on 9 November 2021).
13. Wang, W.; Peng, C.; Kneeshaw, D.D.; Larocque, G.R.; Luo, Z. Drought-induced tree mortality: Ecological consequences, causes, and modeling. *Environ. Rev.* **2012**, *20*, 109–121. [CrossRef]
14. Hislop, S.; Stone, C.; Gibson, R.K.; Roff, A.; Choat, B.; Nolan, R.H.; Nguyen, T.H.; Carnegie, A.J. Using dense Sentinel-2 time series to explore combined fire and drought impacts in eucalypt forests. *Front. For. Glob. Change* **2023**, *6*, 1018936. [CrossRef]
15. Nolan, R.H.; Boer, M.M.; Collins, L.; Resco De Dios, V.; Clarke, H.; Jenkins, M.; Kenny, B.; Bradstock, R.A. Causes and consequences of eastern Australia's 2019–20 season of mega-fires. *Glob. Change Biol.* **2020**, *26*, 1039–1041. [CrossRef]
16. Australian Bureau of Meteorology (BOM). State of the Climate. 2020. Available online: http://www.bom.gov.au/state-of-the-climate/2020/ (accessed on 10 January 2025).
17. Anderegg, W.R.L.; Flint, A.; Huang, C.; Flint, L.; Berry, J.A.; Davis, F.W.; Sperry, J.S.; Field, C.B. Tree mortality predicted from drought-induced vascular damage. *Nat. Geosci.* **2015**, *8*, 367–371. [CrossRef]
18. Adams, H.D.; Zeppel, M.J.B.; Anderegg, W.R.L.; Hartmann, H.; Landhäusser, S.M.; Tissue, D.T.; Huxman, T.E.; Hudson, P.J.; Franz, T.E.; Allen, C.D.; et al. A multi-species synthesis of physiological mechanisms in drought-induced tree mortality. *Nat. Ecol. Evol.* **2017**, *1*, 1285–1291. [CrossRef]
19. Choat, B.; Brodribb, T.J.; Brodersen, C.R.; Duursma, R.A.; López, R.; Medlyn, B.E. Triggers of tree mortality under drought. *Nature* **2018**, *558*, 531–539. [CrossRef]
20. Bendall, E.R.; Bedward, M.; Boer, M.; Clarke, H.; Collins, L.; Leigh, A.; Bradstock, R.A. Mortality and resprouting responses in forest trees driven more by tree and ecosystem characteristics than drought severity and fire frequency. *For. Ecol. Manag.* **2022**, *509*, 120070. [CrossRef]
21. McDowell, N.; Pockman, W.T.; Allen, C.D.; Breshears, D.D.; Cobb, N.; Kolb, T.; Plaut, J.; Sperry, J.; West, A.; Williams, D.G.; et al. Mechanisms of plant survival and mortality during drought: Why do some plants survive while others succumb to drought? *New Phytol.* **2008**, *178*, 719–739. [CrossRef]

22. Climate Change Authority. Sector Pathways Review. Available online: https://www.climatechangeauthority.gov.au/sector-pathways-review (accessed on 10 January 2025).
23. Marusig, D.; Petruzzellis, F.; Tomasella, M.; Napolitano, R.; Altobelli, A.; Nardini, A. Correlation of Field-Measured and Remotely Sensed Plant Water Status as a Tool to Monitor the Risk of Drought-Induced Forest Decline. *Forests* **2020**, *11*, 77. [CrossRef]
24. Jiao, T.; Williams, C.A.; De Kauwe, M.G.; Schwalm, C.R.; Medlyn, B.E. Patterns of post-drought recovery are strongly influenced by drought duration, frequency, post-drought wetness, and bioclimatic setting. *Glob. Change Biol.* **2021**, *27*, 4630–4643. [CrossRef]
25. Jin, S.; Sader, S.A. Comparison of time series tasseled cap wetness and the normalized difference moisture index in detecting forest disturbances. *Remote Sens. Environ.* **2005**, *94*, 364–372. [CrossRef]
26. Hislop, S.; Jones, S.; Soto-Berelov, M.; Skidmore, A.; Haywood, A.; Nguyen, T.H. A fusion approach to forest disturbance mapping using time series ensemble techniques. *Remote Sens. Environ.* **2019**, *221*, 188–197. [CrossRef]
27. Rahman, S.; Mesev, V. Change Vector Analysis, Tasseled Cap, and NDVI-NDMI for Measuring Land Use/Cover Changes Caused by a Sudden Short-Term Severe Drought: 2011 Texas Event. *Remote Sens.* **2019**, *11*, 2217. [CrossRef]
28. Dotzler, S.; Hill, J.; Buddenbaum, H.; Stoffels, J. The Potential of EnMAP and Sentinel-2 Data for Detecting Drought Stress Phenomena in Deciduous Forest Communities. *Remote Sens.* **2015**, *7*, 14227–14258. [CrossRef]
29. Cohen, W.B.; Spies, T.A. Estimating structural attributes of Douglas-fir/western hemlock forest stands from landsat and SPOT imagery. *Remote Sens. Environ.* **1992**, *41*, 1–17. [CrossRef]
30. Tucker, C.J. Red and photographic infrared linear combinations for monitoring vegetation. *Remote Sens. Environ.* **1979**, *8*, 127–150. [CrossRef]
31. Sellers, P.J. Canopy reflectance, photosynthesis and transpiration. *Int. J. Remote Sens.* **1985**, *6*, 1335–1372. [CrossRef]
32. Huete, A.; Didan, K.; Miura, T.; Rodriguez, E.P.; Gao, X.; Ferreira, L.G. Overview of the radiometric and biophysical performance of the MODIS vegetation indices. *Remote Sens. Environ.* **2002**, *83*, 195–213. [CrossRef]
33. Van Wagtendonk, J.W.; Root, R.R. The use of multi-temporal Landsat Normalized Difference Vegetation Index (NDVI) data for mapping fuel models in Yosemite National Park, USA. *Int. J. Remote Sens.* **2003**, *24*, 1639–1651. [CrossRef]
34. Key, C.H.; Benson, N.C. Landscape Assessment (LA): Sampling and analysis methods. In *FIREMON: Fire Effects Monitoring and Inventory System (General Technical Report RMRS-GTR-164-CD*; Lutes, D.C., Keane, R.E., Caratti, J.F., Key, C.H., Benson, N.C., Sutherland, S., Gangi, L.J., Eds.; U.S. Department of Agriculture, Forest Service, Rocky Mountain Research Station: Fort Collins, CO, USA, 2006; pp. LA-1–LA-55.
35. Kennedy, R.E.; Yang, Z.; Cohen, W.B.; Pfaff, E.; Braaten, J.; Nelson, P. Spatial and temporal patterns of forest disturbance and regrowth within the area of the Northwest Forest Plan. *Remote Sens. Environ.* **2012**, *122*, 117–133. [CrossRef]
36. Hislop, S.; Haywood, A.; Alaibakhsh, M.; Nguyen, T.H.; Soto-Berelov, M.; Jones, S.; Stone, C. A reference data framework for the application of satellite time series to monitor forest disturbance. *Int. J. Appl. Earth Obs. Geoinf.* **2021**, *105*, 102636. [CrossRef]
37. Wulder, M.A.; Loveland, T.R.; Roy, D.P.; Crawford, C.J.; Masek, J.G.; Woodcock, C.E.; Allen, R.G.; Anderson, M.C.; Belward, A.S.; Cohen, W.B.; et al. Current status of Landsat program, science, and applications. *Remote Sens. Environ.* **2019**, *225*, 127–147. [CrossRef]
38. Atlas of Living Australia. Australian Citizen Science Project Finder. Available online: https://biocollect.ala.org.au/acsa/project/index/77285a13-e231-49e8-b212-660c66c74bac (accessed on 10 January 2025).
39. Li, P.; Wang, J.; Liu, M.; Xue, Z.; Bagherzadeh, A.; Liu, M. Spatio-temporal variation characteristics of NDVI and its response to climate on the Loess Plateau from 1985 to 2015. *Catena* **2021**, *203*, 105331. [CrossRef]
40. Gibson, R.K.; Hislop, S. Signs of resilience in resprouting Eucalyptus forests, but areas of concern: 1 year of post-fire recovery from Australia's Black Summer of 2019–2020. *Int. J. Wildland Fire* **2022**, *31*, 545–557. [CrossRef]
41. New South Wales Environment and Heritage. NSW Environment and Heritage Website. Available online: https://www.environment.nsw.gov.au/ (accessed on 10 January 2025).
42. Bradstock, R.A.; Gill, A.M.; Williams, R.J. (Eds.) *Flammable Australia: Fire Regimes, Biodiversity and Ecosystems in a Changing World*; CSIRO PUBLISHING: Collingwood, ON, Canada, 2012.
43. Department of Climate Change, Energy, the Environment and Water (DCCEEW). Interim Biogeographic Regionalisation for Australia (IBRA). Available online: https://www.dcceew.gov.au/environment/land/nrs/science/ibra (accessed on 10 January 2025).
44. Prober, S.; Thiele, K.R. Floristic patterns along an east-west gradient in grassy box woodlands of central New South Wales. *Cunninghamia* **2004**, *8*, 306–325.
45. Keith, D.A. *Ocean Shores to Desert Dunes: The Native Vegetation of New South Wales and the ACT*; Department of Environment and Conservation (NSW): Sydney, Australia, 2004.
46. Nguyen, H.T.; Soto-Berelov, M.; Jones, S.D.; Haywood, A.; Hislop, S. Mapping forest disturbance and recovery for forest dynamics over large areas using Landsat time-series remote sensing. In *Remote Sensing for Agriculture, Ecosystems, and Hydrology XIX, Remote Sensing for Agriculture, Ecosystems, and Hydrology*; Neale, C.M., Maltese, A., Eds.; SPIE: Warsaw, Poland, 2017; p. 35. Available online: https://www.spiedigitallibrary.org/conference-proceedings-of-spie/10421/2276913/Mapping-forest-disturbance-and-recovery-for-forest-dynamics-over-large/10.1117/12.2276913.full (accessed on 17 August 2022).

47. Gallagher, R.V.; Allen, S.; Mackenzie, B.D.E.; Yates, C.J.; Gosper, C.R.; Keith, D.A.; Merow, C.; White, M.D.; Wenk, E.; Maitner, B.S.; et al. High fire frequency and the impact of the 2019–2020 megafires on Australian plant diversity. *Divers. Distrib.* **2021**, *27*, 1166–1179. [CrossRef]
48. Giglio, L.; Boschetti, L.; Roy, D.P.; Humber, M.L.; Justice, C.O. The Collection 6 MODIS burned area mapping algorithm and product. *Remote Sens. Environ.* **2018**, *217*, 72–85. [CrossRef]
49. Department of Climate Change, Energy, the Environment and Water (DCCEEW). National Vegetation Information System (NVIS) Version 6.0—Australia. 2018. Available online: https://www.dcceew.gov.au/environment/environment-information-australia/national-vegetation-information-system/data-products (accessed on 10 January 2025).
50. Shang, R.; Zhu, Z. Harmonizing Landsat 8 and Sentinel-2: A time-series-based reflectance adjustment approach. *Remote Sens. Environ.* **2019**, *235*, 111439. [CrossRef]
51. Flood, N. Seasonal Composite Landsat TM/ETM+ Images Using the Medoid (a Multi-Dimensional Median). *Remote Sens.* **2013**, *5*, 6481–6500. [CrossRef]
52. Majasalmi, T.; Rautiainen, M. The potential of Sentinel-2 data for estimating biophysical variables in a boreal forest: A simulation study. *Remote Sens. Lett.* **2016**, *7*, 427–436. [CrossRef]
53. Huo, L.; Persson, H.J.; Lindberg, E. Early detection of forest stress from European spruce bark beetle attack, and a new vegetation index: Normalized distance red & SWIR (NDRS). *Remote Sens. Environ.* **2021**, *255*, 112240.
54. Stone, C.; Kathuria, A.; Carney, C.; Hunter, J. Forest canopy health and stand structure associated with bell miners (*Manorina melanophrys*) on the central coast of New South Wales. *Aust. For.* **2008**, *71*, 294–302. [CrossRef]
55. Urban, M.; Berger, C.; Mudau, T.; Heckel, K.; Truckenbrodt, J.; Onyango Odipo, V.; Smit, I.; Schmullius, C. Surface Moisture and Vegetation Cover Analysis for Drought Monitoring in the Southern Kruger National Park Using Sentinel-1, Sentinel-2, and Landsat-8. *Remote Sens.* **2018**, *10*, 1482. [CrossRef]
56. Xulu, S.; Mbatha, N.; Peerbhay, K.; Gebreslasie, M. Detecting Harvest Events in Plantation Forest Using Sentinel-1 and -2 Data via Google Earth Engine. *Forests* **2020**, *11*, 1283. [CrossRef]
57. Schwalm, C.R.; Anderegg, W.R.L.; Michalak, A.M.; Fisher, J.B.; Biondi, F.; Koch, G.; Litvak, M.; Ogle, K.; Shaw, J.D.; Wolf, A.; et al. Global patterns of drought recovery. *Nature* **2017**, *548*, 202–205. [CrossRef]
58. Jensen, J.R. *Introductory Digital Image Processing: A Remote Sensing Perspective*, 4th ed.; Pearson: Boston, MA, USA, 2016.
59. Han, D.; Liu, S.; Du, Y.; Xie, X.; Fan, L.; Lei, L.; Li, Z.; Yang, H.; Yang, G. Crop Water Content of Winter Wheat Revealed with Sentinel-1 and Sentinel-2 Imagery. *Sensors* **2019**, *19*, 4013. [CrossRef]
60. Brandolini, F.; Domingo-Ribas, G.; Zerboni, A.; Turner, S. A Google Earth Engine-enabled Python approach for the identification of anthropogenic palaeo-landscape features. *Open Res. Eur.* **2021**, *1*, 22.
61. Moreno-Fernández, D.; Viana-Soto, A.; Camarero, J.J.; Zavala, M.A.; Tijerín, J.; García, M. Using spectral indices as early warning signals of forest dieback: The case of drought-prone *Pinus pinaster* forests. *Sci. Total Environ.* **2021**, *793*, 148578. [CrossRef]
62. Wulder, M.A.; Franklin, S.E. (Eds.) *Understanding Forest Disturbance and Spatial Pattern: Remote Sensing and GIS Approaches*; CRC Taylor & Francis: Boca Raton, FL, USA, 2007.
63. White, J.C.; Wulder, M.A.; Hermosilla, T.; Coops, N.C.; Hobart, G.W. A nationwide annual characterization of 25 years of forest disturbance and recovery for Canada using Landsat time series. *Remote Sens. Environ.* **2017**, *194*, 303–321. [CrossRef]
64. Forkel, M.; Carvalhais, N.; Verbesselt, J.; Mahecha, M.D.; Neigh, C.S.; Reichstein, M. Trend change detection in NDVI time series: Effects of inter-annual variability and methodology. *Remote Sens.* **2013**, *5*, 2113–2144. [CrossRef]
65. Verbesselt, J.; Hyndman, R.; Newnham, G.; Culvenor, D. Detecting trend and seasonal changes in satellite image time series. *Remote Sens. Environ.* **2010**, *114*, 106–115. [CrossRef]
66. Moore, C.E.; Beringer, J.; Evans, B.; Hutley, L.B.; McHugh, I.; Tapper, N.J. The contribution of trees and grasses to productivity of an Australian tropical savanna. *Biogeosciences* **2016**, *13*, 2387–2403. [CrossRef]
67. RStudio Team. *RStudio: Integrated Development Environment for R*; RStudio, PBC: Boston, MA, USA, 2023. Available online: http://www.rstudio.com/ (accessed on 10 December 2024).
68. Byer, S.; Jin, Y. Detecting Drought-Induced Tree Mortality in Sierra Nevada Forests with Time Series of Satellite Data. *Remote Sens.* **2017**, *9*, 929. [CrossRef]
69. Aldakheel, Y.Y.; Danson, F.M. Spectral reflectance of dehydrating leaves: Measurements and modelling. *Int. J. Remote Sens.* **1997**, *18*, 3683–3690. [CrossRef]
70. Carter, G.A. Primary and Secondary Effects of Water Content on the Spectral Reflectance of Leaves. *Am. J. Bot.* **1991**, *78*, 916–924. [CrossRef]
71. De Kauwe, M.G.; Sabot, M.E.B.; Medlyn, B.E.; Pitman, A.J.; Meir, P.; Cernusak, L.A.; Gallagher, R.V.; Ukkola, A.M.; Rifai, S.W.; Choat, B. Towards species-level forecasts of drought-induced tree mortality risk. *New Phytol.* **2022**, *235*, 94–110. [CrossRef]
72. Matusick, G.; Ruthrof, K.X.; Fontaine, J.B.; Hardy, G.E.S.J. Eucalyptus Forest shows low structural resistance and resilience to climate change-type drought. *J. Veg. Sci.* **2016**, *27*, 493–503. [CrossRef]

73. Pettorelli, N.; Vik, J.O.; Mysterud, A.; Gaillard, J.-M.; Tucker, C.J.; Stenseth, N.C. Using the satellite-derived NDVI to assess ecological responses to environmental change. *Trends Ecol. Evol.* **2005**, *20*, 503–510. [CrossRef]
74. Keppel, G.; Sarnow, U.; Biffin, E.; Peters, S.; Fitzgerald, D.; Boutsalis, E.; Waycott, M.; Guerin, G.R. Population decline in a Pleistocene refugium: Stepwise, drought-related dieback of a South Australian eucalypt. *Sci. Total Environ.* **2023**, *876*, 162697. [CrossRef] [PubMed]
75. Brown, B.J.; McLaughlin, B.C.; Blakey, R.V.; Morueta-Holme, N. Future vulnerability mapping based on response to extreme climate events: Dieback thresholds in an endemic California oak. *Divers. Distrib.* **2018**, *24*, 1186–1198. [CrossRef]
76. Hammond, W.M.; Williams, A.P.; Abatzoglou, J.T.; Adams, H.D.; Klein, T.; López, R.; Sáenz-Romero, C.; Hartmann, H.; Breshears, D.D.; Allen, C.D. Global field observations of tree die-off reveal hotter-drought fingerprint for Earth's forests. *Nat. Commun.* **2022**, *13*, 1761. [CrossRef]
77. Jiao, T.; Williams, C.A.; Rogan, J.; De Kauwe, M.G.; Medlyn, B.E. Drought Impacts on Australian Vegetation During the Millennium Drought Measured with Multisource Spaceborne Remote Sensing. *J. Geophys. Res. Biogeosciences* **2020**, *125*, e2019JG005145. Available online: https://onlinelibrary.wiley.com/doi/10.1029/2019JG005145 (accessed on 17 August 2023). [CrossRef]
78. Steane, D.A.; Mclean, E.H.; Potts, B.M.; Prober, S.M.; Stock, W.D.; Stylianou, V.M.; Vaillancourt, R.E.; Byrne, M. Evidence for adaptation and acclimation in a widespread eucalypt of semi-arid Australia. *Biol. J. Linn. Soc.* **2017**, *121*, 484–500. [CrossRef]
79. Schnabel, F.; Purrucker, S.; Schmitt, L.; Engelmann, R.A.; Kahl, A.; Richter, R.; Seele-Dilbat, C.; Skiadaresis, G.; Wirth, C. Cumulative growth and stress responses to the 2018–2019 drought in a European floodplain forest. *Glob. Change Biol.* **2022**, *28*, 1870–1883. [CrossRef]
80. Urbazaev, M.; Thiel, C.; Cremer, F.; Dubayah, R.; Migliavacca, M.; Reichstein, M.; Schmullius, C. Estimation of forest aboveground biomass and uncertainties by integration of field measurements, airborne LiDAR, and SAR and optical satellite data in Mexico. *Carbon Balance Manag.* **2018**, *13*, 5. [CrossRef]

Disclaimer/Publisher's Note: The statements, opinions and data contained in all publications are solely those of the individual author(s) and contributor(s) and not of MDPI and/or the editor(s). MDPI and/or the editor(s) disclaim responsibility for any injury to people or property resulting from any ideas, methods, instructions or products referred to in the content.